Article

MMS

Mathematics and Mechanics of Solids
17(4): 364–377

DOI: 10.1177/1081286511420897
mms.sagepub.com

SAGE

A simplified probabilistic macroscopic model for estimating microscopic fracture development in idealized planar fiber network materials

Per Isaksson
The Ångström Laboratory, Uppsala University, Sweden

Received 28 May 2011; accepted 29 July 2011

Abstract
The overall aim of this study is to derive a simplified probabilistic theory to reveal the 'hidden' mechanisms controlling random fracture evaluation in idealized network structures observed as diffuse material failure on the macro scale. The model is based on the classical theory of combinatorics and the practical implications for understanding material failure in network materials, such as non-woven felts made of nanofibers or glass fibers, is addressed. The simplified theory reveals a number of important results regarding the evolution of microscopic fractures in planar random fiber networks where the only active microscopic fracture mechanism is bond fracture and the network is loaded so that a homogeneous macroscopic mechanical field is present. A simple probabilistic expression is derived that estimates the fraction of fractured bonds achieved during the loading history. The equation includes a term for potential energy and assumes that there exists an inherent characteristic bond-strength parameter that is the same for all bonds. Subsequent finite element analyses confirm the simplified probabilistic theory and lend confidence in the rather rough assumptions made. The model is justified by observations in acoustic emission monitored tensile experiments performed elsewhere.

Keywords
bond-energy distribution, fiber network, fracture, homogeneous load

1. Introduction

Living tissues such as bones, muscles and plant stems are examples of natural fiber networks. Manufactured fiber materials are commonly encountered in the automotive and aerospace industries and are used, for example, for filtration processes or medical applications. Traditional paper mainly consists of cellulose fibers, which are about a thousand times larger than fibers in recently developed cellulose nanofibril networks [1]. Common textiles are made of cotton and polyester fibers. Several biomedical implants are currently being developed to mimic the behavior of human tissue. Modern non-woven felts are made of, for example, nanofibers [2] or non-woven glass fibers [3, 4]. Although these materials may, at a first look, appear different they are in fact very similar from a structural point of view: fiber network materials are all composed of structural fibers connected at intersections by bonds.

Corresponding author:
Per Isaksson, The Ångström Laboratory, Uppsala University, Box 534, SE-75121 Uppsala, Sweden
Email: per.isaksson@angstrom.uu.se

The evolution of microscopic fractures, which precedes macroscopic crack growth and ultimate failure, in such materials is a very complex process that depends strongly on the relative volume fraction of fiber and pores, the microstructure (the geometrical arrangement of fiber material, connectivity, thickness, etc.), the mechanical properties of the material constituents and the rates of applied loads. The microscopic fractures can be observed as diffuse material damage on the macroscopic scale. Due to its complex nature, an understanding of fracture processes in network structures is still in its infancy. However, from mechanical experiments on fiber-based materials it is well known that a material experiences microscopic fracture in the form of bond or fiber breakage. In cases where the bonds connecting the fibers are weak or moderately strong, in comparison to the fibers, bond fracture is the most likely microscopic fracture mechanism in a network structure subjected to mechanical load [5].

In previous studies, the initial creation of diffuse microscopic fractures has often been approached by modeling networks of interlinked uniaxial structural elements, with a condition on the bond or fiber break threshold. The history of the model is followed as the imposed macroscopic strain is increased. The fracture formation process has been studied numerically, among others, see [6] and [7]. Often, parameter studies have been performed to reveal the influence of various micro-level parameters on the geometry of the structure and the elastic stiffness on the macro level. A numerical analysis [7] has shown, assuming bond breakages are the prevailing micro-fracture mechanism, that above a certain density limit (percolation), the development of global macroscopic elastic degradation follows an exponential law controlled by a bond fracture rate parameter. There are several different starting points for the mechanical analysis of network materials; micromechanical models have the distinct advantage of being able to capture structural details at the micro scale and of permitting formulation of the kinetic equation for fracture evolution based on the physical process involved; among others, see [8]. However, due to the complexity of the microstructure in fiber networks, fracture evolution laws based on micromechanical models are difficult to develop with adequate accuracy. An alternative starting point is in the theory of statistical mechanics. Among others, Mishnaevsky [9] has reviewed damage and fracture theories derived from statistical mechanics. A similar approach, although novel and somewhat simplified, for estimating fracture processes in networks is applied here. The aim is to derive a simplified probabilistic theory to reveal the 'hidden' mechanisms controlling fracture evaluation in idealized random fiber network structures. Understanding the fracture behavior of such structures brings important insights about how many types of fiber materials, such as paper materials and short-fiber composites, behave. Attention is confined to a purely probabilistic mechanical theory assuming quasi-static loading conditions. Fiber-to-fiber bond fracture is considered as the only active fracture process and the threshold for the bond strain energy is assumed to govern fracture evolution.

The simplified probabilistic theory is illustrated with observations from acoustic emission assisted experiments on a sparse fiber-based material and compared with finite element models.

2. Theory

2.1. General assumptions

The overall aim for this study is to reveal hidden mechanisms controlling fracture evolution in idealized network structures. This means that some heavy simplifications are made but it is the author's belief that the primary underlying mechanism is not violated. Consider a planar random fiber network as illustrated in Figure 1. The analysis is restricted to two-dimensional structures, that is, in-plane mechanical behavior, and attention is confined to a purely probabilistic mechanical theory. The body is mechanically loaded in tension so that in an average sense a homogeneous macroscopic stress field σ and a homogeneous macroscopic elastic strain field ε are present. The fiber network is further understood to have in-plane isotropic material behavior on the macroscopic scale and it is for simplicity assumed that the material could be described by a small deformation theory. To further simplify matters, the fibers in the network are highly idealized. This means that the network consists of, in total, N_F linearly elastic fibers with unit thickness and length L, width h and Young's modulus E_F. The

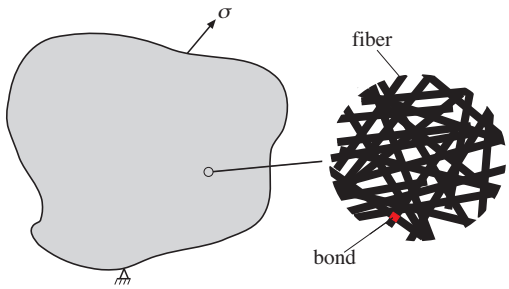

Figure 1. Mechanically loaded fiber network.

unit area of the macroscopic network is A and each microscopic bond has a characteristic bond area A_b. The average of the total number of bonds N in a network is given by [10]:

$$N = N_F^2 L^2/[\pi A], \tag{1}$$

which completely specifies the planar random fiber network. Supported by experimental observations [5], microscopic bond fractures may nucleate when the network is subjected to increasing load. This progressive physical microscopic process of degradation of the mechanical properties up to complete failure is commonly referred to as diffuse damage on the macroscopic scale. Herein, a clear distinction is made between 'damage' and 'plasticity'. In the context of fiber-based materials it is convenient to define a damage process as the irreversible process where either a fiber or a fiber-to-fiber bond breaks, while a plastic process is when there is an irreversible straining of the fibers themselves. However, for the network materials discussed here, it is assumed that there is no significant amount of plastic deformation of the fibers since they are considered stiff with a high yield stress. This is motivated by the observation that since the bonds are assumed weak in comparison to the fibers, a relatively low axial stress field is present in the fibers prior to breakage. In this case plasticity would be a critical factor only if the fibers were very soft.

It is further assumed that the loading process of the network is carried out slowly, so that the macroscopic system remains arbitrarily close to equilibrium at all stages of loading. Hence, the network is considered quasi-static: the potential energy Π of the system is well defined and estimations of stress σ and strain ε can be obtained by established theories of mechanics. Naturally, since the system is considered quasi-static, all dynamic effects are neglected and it is anticipated that a bond fracture will not instantly trigger fractures in neighboring bonds resulting in simultaneous 'bursts'. However, due to the redistribution of forces in the network when a bond fractures, all remaining bonds are of course indirectly affected but this is considered a slower process in time and is a motivation for the assumed quasi-static mechanical behavior.

2.2. *Bond-energy distribution*

When the network becomes loaded, the N randomly distributed bonds will possess different strain energies as a result of their random positions in the system. Only bond energies are taken into account. Thus, the fibers are assumed to be only load carriers and are not inclined to fracture. Observing that the bonds in the network can be considered as identical – but distinguishable – particles since they have equal volumes, the distribution of the bond strain energies in the system can be estimated using the well-known exponential Maxwell–Boltzmann distribution. A very good educational introduction to the subject can be found in the instructional material on the site *HyperPhysics*, developed by Carl R. Nave [11], but also in any classical textbook on statistical physics such as [12] or [13].

The exponential distribution seems to be a general property of disordered materials where the disorder arises from randomly distributed pores (among others, see [14] and [15]). Knowing this, it seems reasonable to adopt an exponential distribution to describe the bond energies present in a fiber network. This observation is also a

Table 1. Calculated results for the example when $N = 5$. n_{ij} is the number of bonds within energy region j in distribution i.

	$W_j \in \{0 \pm \frac{1}{2}\}\Delta w$	$W_j \in \{1 \pm \frac{1}{2}\}\Delta w$	$W_j \in \{2 \pm \frac{1}{2}\}\Delta w$	$W_j \in \{3 \pm \frac{1}{2}\}\Delta w$	$W_j \in \{4 \pm \frac{1}{2}\}\Delta w$	m_i	$m_i/\sum_i m_i$
n_{ij} (i=1)	4				1	5	5/70
n_{ij} (i=2)	3		2			10	10/70
n_{ij} (i=2)	3	1		1		20	20/70
n_{ij} (i=3)	2	2	1			30	30/70
n_{ij} (i=4)	1	4				5	5/70
n_j	175/70	100/70	50/70	20/70	5/70		

principal reason why Cox's network formulation [16] from 1952 is insufficient for this type of analysis since that theory assumes a homogeneous strain field on the microscopic scale also. Now, consider a homogeneous loaded network structure consisting of N bonds. Let the total bond strain energy in the system be W_{tot} (i.e., the sum of all the bond energies present in the network is W_{tot}). All possible divisions of individual bond energies W are assumed to occur with the same probability as a result of the randomly positioned bonds. However, since the bonds are randomly positioned in the system it is likely that individual bond energies will differ throughout the system and an appropriate probability theory has to be included. For mathematical reasons, assume that each bond can possess a strain energy W that is within one of the N discrete energy regions determined by $\{j - \frac{1}{2}, j + \frac{1}{2}\}\Delta w$ where $j = 0, 1, \ldots, N - 1$ and $\Delta w = W_{\text{tot}}/[N - 1]$. Notice that the factor $N - 1$ is because the bonds may be unloaded, that is, have zero energy. The width of the N energy regions is determined by Δw, which shrinks as $N \to \infty$.

It is necessary to calculate the number of different ways each energy field distribution can be produced with the constraint that the sum of all bond strain energies is equal to W_{tot}. There is no restriction on the number of bonds that can be in a certain strain energy region W_j. As well as the number of bonds in each energy region, it is important to know which bonds are in each region. The first step is to count the number of possible ways to obtain the sum W_{tot} for different total numbers of i bonds carrying the load. Then, making use of the classical theory of combinatorics, the number of distinguishable ways m_i to obtain each possible distribution i is given by

$$m_i = \frac{N!}{n_{i1}!n_{i2}! \cdots n_{iN}!} \tag{2}$$

where n_{ij} is the number of bonds in energy region j in distribution i. To establish a distribution function for the number of bonds in each energy region, the number of bonds is weighted over all possible m_i according to:

$$n_j = \frac{\sum_i n_{ij} m_i}{\sum_i m_i}. \tag{3}$$

To illustrate how an exponential distribution can be estimated for a network, a simple ('school book') example of a network structure consisting only of five bonds ($N = 5$) is presented in Table 1.

Figure 2 shows the calculated (Table 1) estimated average population n_j at discrete energies W_j/W_{tot}. Now, plotting n_j as a function of W_j/W_{tot}, the exponential energy distribution is obtained,

$$n_j = C \exp(-bW_j/W_{\text{tot}}), \tag{4}$$

where C and b are physical constants that will be discussed further below. In (4) it can be seen that the fraction W_j/W_{tot} is independent of Δw. In Figure 2 a line is drawn that is fitted in a least-squares sense according to (4) using the calculated values in Table 1, utilizing the center of each region. Obviously, as $W_j/W_{\text{tot}} \to 1$ the distribution of energies will always have a cutoff since n_j is discrete but this has limited effect on this simplified theory since almost all bonds will have low energies throughout the network. As observed in Figure 2, lower energies are statistically favored because there are more ways to get them. If a single bond has a high-energy level, then it reduces the number of possibilities for the distribution of the remainder of the energy since the

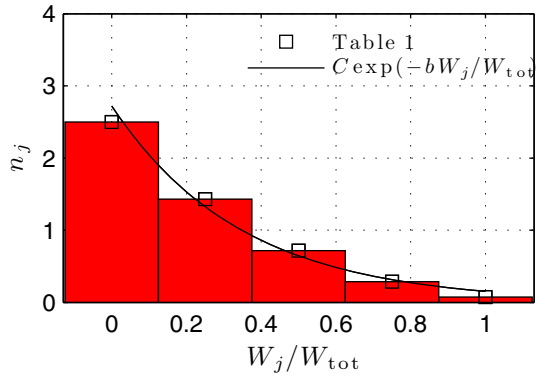

Figure 2. Probability distribution for $N = 5$. n_j is the estimated average number of bonds having energy level $W_j/W_{\rm tot}$ from Table 1. The line represents an exponential distribution and is obtained by a least-squares fit. For simplicity, the values belonging to a specific energy region are placed in the center of that region.

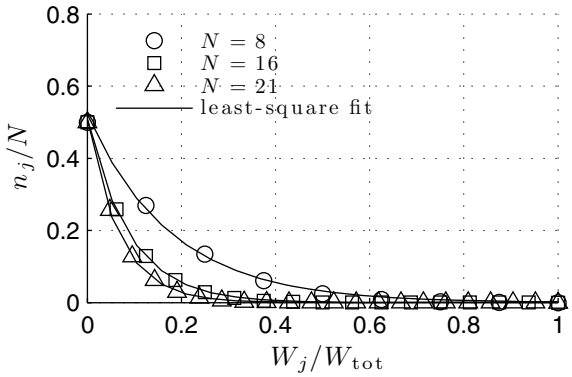

Figure 3. Calculated probability distributions n_j/N for three different values of N. A least-squares fit, according to (4), is also show for each value of N.

sum of all bond energies is constrained to be constant. Thus, with increasing energy W_j it is progressively less likely that any given bond will attain that specific energy region, meaning that more bonds will be found with lower energies.

As illustrated in this simple example, the derivation of the exponential distribution in a general analytical form is a tough mathematical task. However, the author has computed the distributions for n_j up to $N = 21$. Notable is that even though 21 is a fairly low number, the computations took several weeks to perform with a highly optimized Fortran code on a modern computer.

The probability distributions n_j/N for $N = 8$, 16 and 21 are displayed in Figure 3. The numerically estimated constant b, fitted in a least-squares sense according to (4), is shown in Figure 4 for each N computed. The least-squares fit reveals that $b \approx 0.693N$ while from Figure 3 it is obvious that C has the value $N/2$. Based on the numerical results shown in Figures 3 and 4, it is assumed that the relations $C = N/2$ and $b \approx 0.693N$ hold even when $N \to \infty$ (and $\Delta w \to 0$). Obviously, the constants C and b uniquely determine the energy field distribution of all the bonds present in the network. One should bear in mind that this derived probabilistic theory, based on classical combinatorics, has several severe simplifications but it should nevertheless reveal important information and provide answers regarding material degradation in this class of network materials.

2.3. Linking macroscopic potential to microscopic strain energy

Bearing in mind the assumption that the fibers in the network are considered linearly elastic and are undergoing small deformations, one realizes that the microscopic strain energy for any bond and the total macroscopic

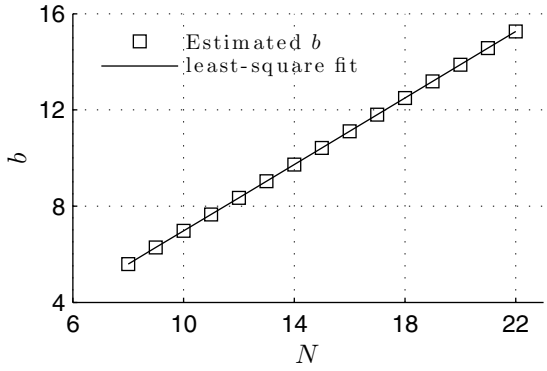

Figure 4. Numerically estimated constant b calculated for each N. The least-squares fit reveals $b \approx 0.693N$.

potential energy Π of the system scale linearly even though the bond energies are exponentially distributed and the fibers in the network possess substantial amounts of strain energy. As long as small strain prevails, the ratio between the sum of bond strain energies and the sum of fiber strain energies is preserved regardless of the magnitude of the applied load for the same load configuration. If the potential energy Π in the body increases, the individual bond energies increase in a relatively equal amount provided that no bonds fracture. This linear behavior is a consequence of the mechanical assumptions made and arises from the fact that the macroscopic potential energy is equal to the sum of all the individual structural (bonds and fibers) element energies present in the system when the body is at rest and force equilibrium prevails. Now, let Π_0 denote a scaling material parameter determined in such a way that the ratio $\Pi_j/\Pi_0 = 1$ when $W_j/W_{\text{tot}} = 1$ and $\Pi_j/\Pi_0 \to \infty$ when $W_j/W_{\text{tot}} \to 0$. Then the following inversely proportional relation holds:

$$\frac{W_j}{W_{\text{tot}}} = \frac{\Pi_0}{\Pi_j}. \tag{5}$$

2.4. Estimation of bond fracture evolution

Since the material is considered linearly elastic, the energy for bond fracture growth is the specific surface energy γ to form two new free surfaces, that is $W = 2\gamma A_{\text{b}}$. The specific surface energy γ is a material property. Hence, it is here assumed that a bond fractures if the available strain energy W in the bond exceeds a threshold value $\lambda = 2\gamma A_{\text{b}}$. With this assumption, one realizes that, since the distribution (4) is known, it is possible to obtain a rough estimate of the number of bonds that fracture at a certain level of load $\Pi_j \geq \Pi_0$ by combining (4) and (5),

$$n_j = C \exp(-b\Pi_0/\Pi_j). \tag{6}$$

Equation (6) may seem far too simplistic. However, it has physical relevance. As illustrated by the author in a previous study [7], the exponential distribution of bond energies in a network does not change significantly during a loading/fracture process, except when the ratio between broken and unbroken bonds approaches 1 when localization take place. During the loading process, some bonds activate while some break, but this process will only result in an insignificantly small change of the global bond strain energy distribution in the network and can be kept at a constant level without severe loss of information. The bonds that become activated are mainly in the lower energy regime in the network and are almost unloaded, while those which break are in the higher energy regimes and consequently have a significant impact on the global degradation of the network's macroscopic stiffness. With this in mind one realizes that the simplified estimate of (6) can be considered fair for the circumstances discussed here. Observing that the relation between infinitesimally small energy changes

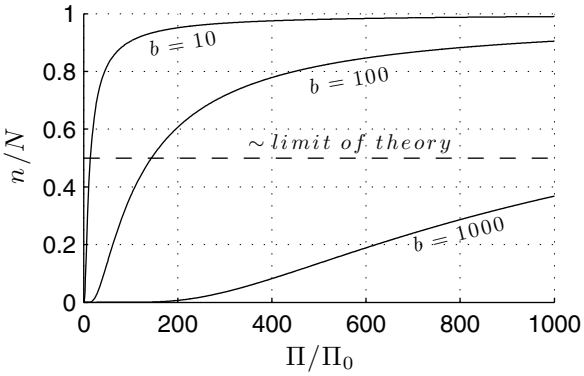

Figure 5. Estimated microscopic fracture ratio n/N versus macroscopic energy Π/Π_0. A dashed line indicates a limit for the theory.

of W and Π is $dW \propto -d\Pi/\Pi^2$, according to (5), an estimate of having, in total, n fractured bonds out of a total of N bonds per unit area A at a specific energy level $\Pi \geq \Pi_0$ is given by

$$\frac{n}{N} = \frac{\int_{\Pi_0}^{\Pi} \tau^{-2} \exp(-b\Pi_0/\tau) d\tau}{\int_{\Pi_0}^{\infty} \tau^{-2} \exp(-b\Pi_0/\tau) d\tau}, \tag{7}$$

where the normalizing denominator is taken as the integral over all states of the system and τ is an integration dummy. The solution to (7) in the macroscopic energy regime $[\Pi_0, \Pi]$ yields (for $N \gg 1$)

$$\frac{n}{N} = \frac{\exp(-b\Pi_0/\Pi) - \exp(-b)}{1 - \exp(-b)} \approx \exp(-b\Pi_0/\Pi). \tag{8}$$

Needless to say, for situations when $\Pi < \Pi_0$ the network remains unfractured. It can also be observed from (8) that when $\Pi/\Pi_0 = 1$, $n/N = 0$ while when $\Pi/\Pi_0 \to \infty$, $n/N \to 1$. The region where the theory is reasonably accurate is $0 \leq n/N \lesssim 1/2$. When applying (8), be aware that the potential energy Π is for an unfractured network. The energy Π should be understood as an effective potential energy parameter that reflects the energy that an unfractured network should have at the same load level as a fractured one. This is because (8) is based on the virgin energy distribution and not the actual distribution where n bonds have fractured. As discussed above, when bond fractures evolve, the number of load-carrying bonds is assumed approximately constant throughout the load regime at which (8) is valid. It is also understood that even though the change of the global bond strain energy distribution in the network is vanishingly small during the bond fracturing process, a single bond fracture leads to a change in the network's potential energy that may be substantially larger than the bond fracture energy λ. The reason for this phenomenon is a relaxation effect of fibers in the region surrounding the fracture site in the network and that energy may dissipate out of the system during the fracture process. However, this drop in potential energy is several orders of magnitude lower than the total energy in the network and is disregarded in this simplified analysis.

Figure 5 shows the estimated cumulative fracture ratio n/N as function of the macroscopic strain energy Π/Π_0 according to (8) for three different values of b. It can be seen that the rate of bond fracture is significantly different at low values of n/N. However, the three networks have different fiber and bond densities and, therefore, totally different macroscopic properties such as Young's modulus and material energy parameter Π_0.

2.5. Experimental illustration

Equation (8) is an estimate of the total number of bonds fractured in the global load regime $[\Pi/\Pi_0 \geq 1]$. However, how well does relation (8) describes what is actually observed? Work carried out earlier has shown that the way stochastic fiber network materials, such as sparse tissue, fractures in tensile experiments can be

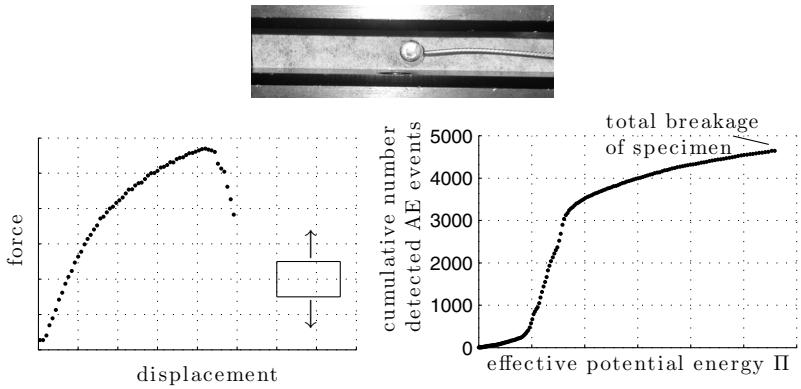

Figure 6. (Upper) An acoustic sensor is held fixed on the specimen with a magnetic holder located on the remote side of the specimen. The diameter of the sensor is 3 mm and the sensor is encapsulated in a shelter having a diameter of 6 mm. (Lower, left) Force-displacement test and (lower, right) simultaneously measured acoustic emission (AE) activity during a tensile test performed on a specimen made of a sparse in-plane isotropic cellulose fiber material. It is understood that each detected event stems from a bond fracture in the vicinity of the sensor.

followed by acoustic sensors and that the measured signals are closely related to the fracture processes occurring within the material's structure, see [17] or [18]. The basic principle is that during a bond fracture (which will occur in microseconds), stresses in a neighborhood of the fracture site will be redistributed and cause a rapid release of elastic energy, which is transmitted through the material as an elastic wave that can be recorded on the surface of the material using an appropriate acoustic emission sensor (Figure 6). In this way each fracturing of a bond is the source of one acoustic emission event. Previously, the author has performed acoustic emission monitored experimental studies on a sparse isotropic cellulose fiber tissue material, specially designed to ensure bond fracture is the dominating fracture mechanism [5]. Figure 6 shows a typical force-displacement curve and the acoustic response as a function of the effective potential energy Π estimated for the same test. One may observe that the shape of the acoustic emission curve is very similar to the results in Figure 5. This typical behavior will be employed in the next section to estimate the material energy parameter Π_0.

2.6. Estimation of energy parameter Π_0

Taking the derivative of (8) with respect to energy Π gives the estimated bond fracture rate ($N \gg 1$):

$$\frac{d(n/N)}{d\Pi} = \frac{b\Pi_0 \exp(-b\Pi_0/\Pi)}{\Pi^2}. \tag{9}$$

Now, let Π^* denote the effective potential energy at the inflection point, that is, Π when $d^2(n/N)/d\Pi^2 = 0$. Taking the derivative of (9) and finding the root gives

$$\Pi_0 = 2\Pi^*/b. \tag{10}$$

From equation (10), the energy parameter Π_0 can be estimated in acoustic emission assisted experiments as in Figure 6 (since $b \approx 0.693N$ is a known quantity). It should be possible after a series of experiments to localize an approximate position of the inflection point and, in turn, Π^*. From a mathematical view, the exact position of Π^* is at the fracture ratio $n/N = \exp(-2) \approx 0.135$, see Figure 5, which is well below the limit $n/N \approx 1/2$. However, since the acoustic events are detected in a diffuse region in the vicinity of the sensor, it is difficult to obtain a direct relationship between the global fracture ratio n/N and the detected acoustic events.

3. Finite element analysis

To assess the probabilistic theory developed, the evolution of bond fractures in a two-dimensional random fiber network was analyzed using a finite element model. When putting together a finite element network model one

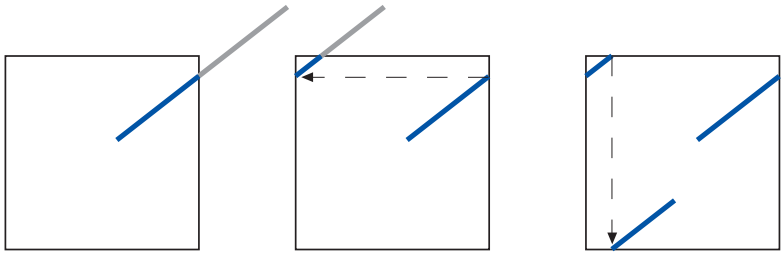

Figure 7. Illustration of fiber modification to ensure that fiber and bond densities are similar over the network and have a periodic arrangement. The quadratic domain has unit area *A*. The fiber is cut at the boundaries and the detached piece is moved one side-length and placed within the domain. This procedure is repeated until all fiber parts are located within the domain.

need to be cautious about the physical limitations of the element formulations. It is well known that if the ratio between segment length (distance between adjacent bonds) and segment width is $\gtrsim 10$, the classical Euler–Bernoulli's engineering beam theory is satisfactory while for shorter segment lengths, Timoshenko engineering beam theory may be used [19]. Here the model uses two-dimensional first-order linear-elastic Timoshenko beams that can be stretched and bent.

A quadratic domain (unit-cell) of size A, with unit thickness, subjected to a monotonically increasing nominal macroscopic tensile strain is analyzed. To ensure that the fiber and bond densities are evenly distributed over the network, some precautions are introduced when generating the networks. With reference to Figure 7, the fiber sections that extend outside the quadratic domain in the mesh generation procedure are moved one side-length in the preferred direction and so located inside the problem domain.

To further simplify matters, the fibers are assumed to have a rectangular cross section and elastically coupled at each intersection by a very stiff (relative to the fiber structural element) spring element in order to calculate the elastic strain energy stored in individual bonds. Further, for simplicity, the spring elements representing the bonds are assumed to have circular domains with a diameter equal to the fiber width and vanishing thickness. The connection represents stiffness against relative motion between connected fibers in both translation and rotation. A mathematical description of the structural bond element utilized is given in the appendix.

The model is solved using well-established finite element algorithms for small deformation theory. The numerical scheme is implemented in a MATLAB [20] code. The intention is to create an approximately homogeneous strain field on the macroscopic level. A type of periodic straight boundary condition was applied, which simulates the response of a unit cell of the material when a small piece of the material is subjected to uniaxial loading. The routine incrementally increases the nominal strain of the system by applying a uniform prescribed displacement along one horizontal boundary while the opposite horizontal boundary is restrained from moving in the loading direction. The vertical boundaries are restrained straight throughout loading even though they can move freely in the vertical direction. The rotational degrees of freedom are restrained along the boundaries to fulfill the condition of periodic straight boundary conditions.

The network is considered quasi-static; hence, the potential energy of the system is well defined and the total reaction forces and displacements of the boundaries determine the estimates of the macroscopic stress and strain at each load increment. Bond failure is the only fracture mechanism considered and an energy criterion is used to control bond failure. A bond break occurs in the model when the elastic strain energy stored in a bond element between two fiber structural elements is sufficient to overcome a threshold resistance λ, which is equal for all bonds. The bond threshold represents every dissipation process associated with breaking a fiber bond. Modeling the bonds as structural elements allows one to easily compute the elastic strain energy stored in the bonds by standard methods in the finite element framework. For numerical efficiency, all bond elements that exceed the threshold energy (i.e. those that are fractured) are in subsequent computations erased by setting their stiffness to zero in the global stiffness matrix. Thereby the fibers at the broken intersections are allowed to move in an unrestrained manner without the need for an updating routine for the network mesh since small deformations are assumed to prevail.

The finite element network model was used to investigate a number of networks having different inherent properties (fiber and bond densities, fiber length and width, etc.). In all fiber networks considered, the fiber

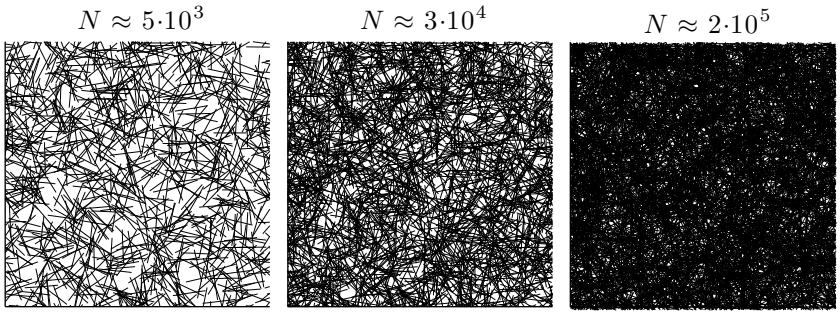

Figure 8. Examples of networks having relatively low, medium and high densities. In all cases, L/h=100 and $A = (L/8)^2$.

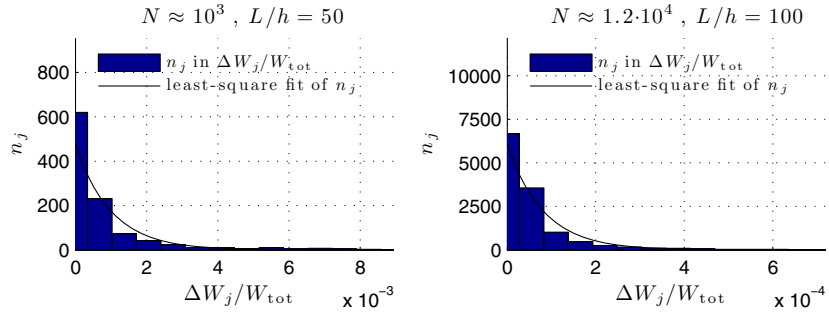

Figure 9. Typical bond-energy distributions computed with the finite element model. n_j is the number of bonds with strain energy in the region $\Delta W_j/W_{\rm tot}$, where ΔW_j is $(j \pm \frac{1}{2})W_{\rm tot}/N$, $j = 0, 1, \ldots, N-1$. The unit area in the two examples is $A = (L/4)^2$ (left) and $A = (L/8)^2$ (right).

length-to-width ratio, that is, the aspect ratio, is $L/h = 50$ or $L/h = 100$. The number of fibers $N_{\rm F}$ is varied and the quadratic unit area A of the problem domain is in the range $(L/8)^2$ to $(L/2)^2$. For each set of inherent properties, 10 different networks were produced (i.e. with different seeds in the random generator) to allow for stochastic variations in the analysis. Examples of planar networks of various densities are shown in Figure 8. In total, around a thousand unique networks were analyzed.

3.1. Analysis of pre-fracture bond-energy distribution

The histograms in Figure 9 show the distribution among the bond strain energies in two typical network configurations, calculated with the finite element model. The networks are loaded in such a way that no bonds have fractured and the strain energies are normalized with the sum of all bond energies in the respective network. The results in Figure 9 should be compared to those presented earlier in Figures 2 and 3. Also drawn in Figure 9 are fitted exponential curves. For illustrative purposes, only the regions of low energies are displayed.

According to this result it seems as if the finite element models confirm the observation from Figure 2 that the strain energy distribution among the bonds in a network follows an exponential distribution. As discussed for Figure 2, and illustrated in Figure 9, lower energies are statistically favored because there are more ways to get them. If a single bond has a high energy, then it reduces the number of possibilities for the distribution of the remainder of the energy. This is a result of the normalization with the sum of all bond energies. To further explore this observation, the parameter b in equation (4) is studied. Figure 10 shows the least-squares fitted parameter b for numerous finite element analyzed networks of different sizes and densities.

The fiber-to-width ratios utilized here are $L/h = 100$ and $L/h = 50$. The fitted straight line (in a least-squares sense) is $b = 0.709N$, which is $\sim 1\%$ from the corresponding value $b = 0.693N$ numerically estimated in Section 2.

A similar result is shown in Figure 11. However, in contrast to Figure 10, the macroscopic tensile load on the networks is here biaxial. The networks producing the result in Figure 11 are loaded by applying the prescribed

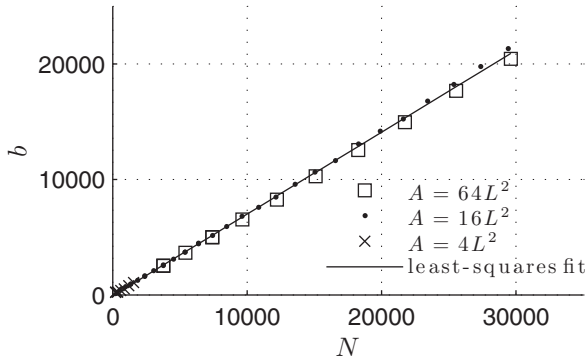

Figure 10. Numerically estimated b for several different networks. Each mark corresponds to the average value of b estimated for 10 different networks having equal inherent properties (average fiber/bond density, fiber length/width).

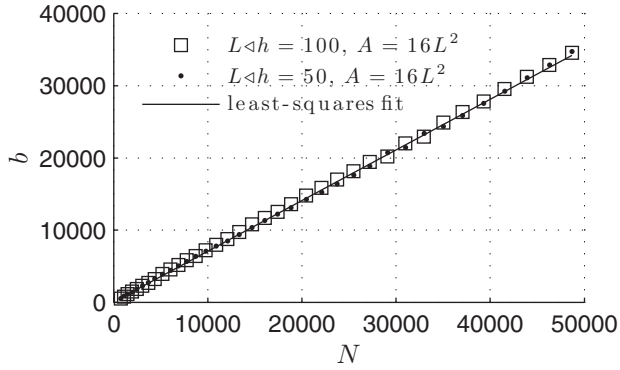

Figure 11. Numerically estimated b for several different biaxially loaded networks. As in Figure 10, each mark corresponds to the average value of b estimated for 10 different networks having equal inherent properties (average fiber/bond density, fiber length/width).

normal displacements, equal in magnitude, simultaneously along one horizontal boundary and one vertical boundary while their opposite boundaries are restrained from moving. Obviously, the resulting macroscopic stress field is also, in this loading situation, homogeneous. As can be observed from Figure 11, much the same result is estimated ($b = 0.702N$), which reveals that a similar energy distribution is present. A conclusion one can draw, with support from Figures 10 and 11, is that as long as the macroscopic field is homogeneous, the bond energies seem to have an exponential distribution with the exponent $b \approx 0.693N$ according to the theory outlined in Section 2. This observation lends some confidence to the simplified theory discussed here.

3.2. Note on bond fracture evolution

The material energy scaling parameter Π_0 can be estimated by analyzing the fracture rate in the network during increasing load and applying equation (10). This may be done, for example, in acoustic emission assisted experiments.

Figure 12 shows typical curves obtained from the numerical simulations.

Since the fracture ratio n/N is known from the finite element model, the energy parameter Π_0 can be readily determined in each network configuration directly within the analysis by picking $\Pi^* = \Pi$ when $n/N = \exp(-2)$ and using equation (8) together with the theoretical estimate $b = 0.693N$.

The macroscopic energy parameter Π_0 is obviously related to the networks' inherent properties and cannot be derived theoretically. However, the fracture rate can, in general terms, be discussed. Figure 13 shows a comparison for three network configurations. Networks 1 and 2 have equal bond density ($N \approx 2 \times 10^4$) but

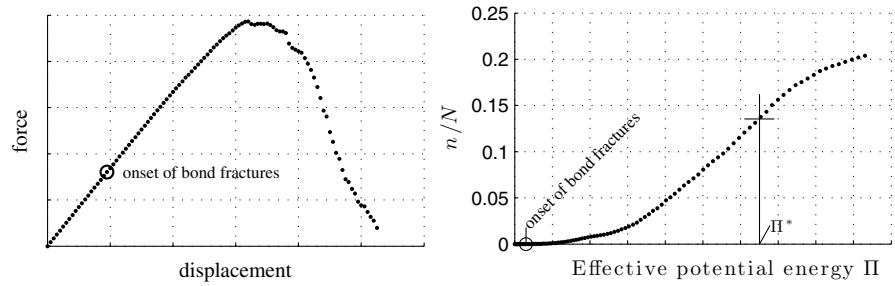

Figure 12. Typical results from a fracturing network. (Left) Force-displacement relation. (Right) Fractured bond ratio n/N as a function of the effective potential energy Π in the network. The inflection point and the corresponding energy Π^* are indicated. The geometric configuration is $N \approx 1.6 \times 10^4$, $L/h = 100$ and $A = 16L^2$.

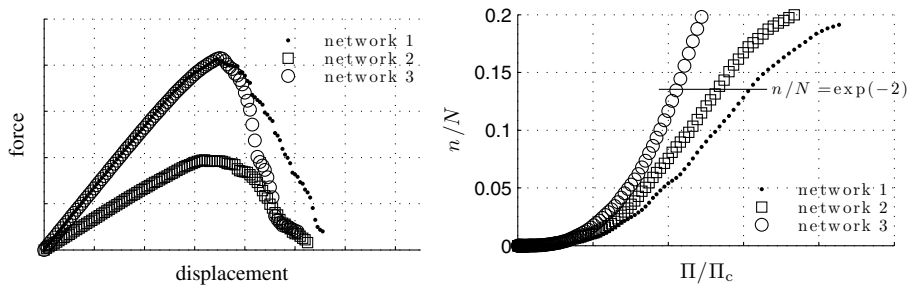

Figure 13. Comparison of the fracture rate for three different networks ($A = 16L^2$). For the sake of transparency, the effective energy Π is normalized with the energy Π_c, which is the (macroscopic) potential energy when the first bond fracture nucleates in the respective network and should not be confused with Π_0. Hence, the ratio Π/Π_c reflects the relative effective energy required to obtain n/N bond fractures. (Right) The position of $n/N = \exp(-2)$ is indicated by a straight line.

their fiber length-to-width ratios are different ($L/h = 50$ and $L/h = 100$, respectively). Naturally, the network having wider fibers has the higher stiffness because of the larger load-carrying area in the network. Network 3 has slender fibers ($L/h = 100$) while its density is approximately twice as high ($N \approx 5 \times 10^4$), so that its stiffness is similar to network 1's stiffness since the magnitude of fiber coverage is equal. As can be seen in Figure 13, the network with slender fibers has relatively higher fracture rates than the network with relatively wider fibers. When bonds start to break, the amount of macroscopic potential energy needed to obtain more breaks is relatively smaller for networks having slender fibers than for networks having wider fibers. Hence, for networks with the same bond densities, the rate of bond fractures is expected to be relatively higher for high fiber length/width ratios than for lower ratios, which can be concluded from Figure 13. Thus, networks with lower fiber length/width ratios fracture more slowly and can, therefore, be considered as tougher in a fracture sense. A conclusion is that the material energy parameter Π_0, which can be estimated experimentally using equation (10), is a scaling parameter that determines how separated the individual bond energies are in the system.

4. Conclusions

The mechanical behavior of fiber networks is governed by complex multiple mechanisms. The overall aim of this study was to derive a simplified probabilistic theory to reveal the 'hidden' mechanisms controlling fracture evaluation in idealized network structures observed as diffuse material failure on the macro scale. A classical theory of combinatorics was applied. The practical implications for understanding material failure in network materials, such as non-woven felts made of nanofibers or glass fibers, were addressed. The fibers are randomly distributed in the network meaning that the network has in-plane isotropic properties on the macroscopic scale. Various networks, with different inherent properties (fiber and bond density, fiber length and width, etc.), were loaded in such a way that, in an average sense, homogeneous macroscopic stress and strain fields were present.

Even though a large number of simplifications were made, the analysis reveals a number of important results regarding the evolution of microscopic random fractures in planar random fiber networks where the only active microscopic fracture mechanism is bond fracture.

- According to the simplified probabilistic theory, the strain energy stored in interfiber bonds over the whole network seems to follow an exponential distribution given by $n_j \approx \frac{N}{2}\exp(-0.693NW_j/W_{\text{tot}})$, where n_j is the estimated number of bonds possessing strain energy W_j while W_{tot} is the sum of the strain energies for all of the N bonds. This behavior was assessed and confirmed in finite element models for numerous network configurations.
- A probability equation was derived, based on classical combinatorics, that estimates the development of the total n bond fractures in the network assuming that there exists an internal characteristic bond-strength material parameter that is equal for all bonds in the particular network. Assuming $N \gg 1$ the simplified expression reads $n/N \approx \exp(-0.693N\Pi_0/\Pi)$, where $\Pi \geq \Pi_0$ is the effective potential energy of the network and Π_0 is a material energy parameter that can be estimated from acoustic emission monitored experiments and scales the separation of the individual bond strain energies in the system. A limit for the simplified theory is $n/N \sim 1/2$.
- Using a knowledge of the estimated probabilistic debond ratio n/N, the development of random diffuse macroscopic material failure can be estimated since the ratio reflects a decrease of the internal load-carrying area of the network and, hence, a reduction of the network's global stiffness.
- The simplified probabilistic theory has been confirmed by observations in acoustic emission monitored tensile experiments performed elsewhere.

Funding

This work was supported by the Swedish Research Council [grant number 2007–4565].

Conflict of Interest

None declared.

References

[1] Henriksson, M, Berglund, LA, Isaksson, P, Lindström, T and Nishino, T. Cellulose nanopaper structures of high toughness. *Biomacromolecules* 2008; 9: 1579–1585.
[2] Dzenis, Y. Spinning continuous fibers for nanotechnology. *Science* 2004; 304: 1917–1919.
[3] Ridruejo, A, González, C, and Llorca, J. Damage micromechanisms and notch sensitivity of glass-fiber non-woven felts: An experimental and numerical study. *J Mech Phys Solids* 2010; 58: 1628–1645.
[4] Ridruejo, A, González, C, and Llorca, J. Micromechanisms of deformation and fracture of polypropylene nonwoven fabrics. *Int J Solids Struct* 2011; 48: 151–162.
[5] Hägglund, R, and Isaksson, P. Analysis of localized failure in low-basis weight paper. *Int J Solids Struct* 2006; 43: 5581–5592.
[6] Heyden, S, and Gustafsson, PJ. Simulation of fracture in a cellulose fibre network. *J Pulp Paper Sci* 1998; 24(5): 160–165.
[7] Hägglund, R, and Isaksson, P. On the coupling between macroscopic material degradation and interfiber bond fracture in an idealized fiber network. *Int J Solids Struct* 2007; 45: 868–878.
[8] Maire, JF, and Chaboche JL. A new formulation of continuum damage mechanics (CDM) for composite materials. *Aero Sci Tech* 1997; 1(4): 247–257.
[9] Mishnaevsky, LL. Methods of the theory of complex systems in modeling of fracture: A brief review. *Engng Frac Mech* 1997; 56(1): 47–56.
[10] Corte, H, and Kallmes, OJ. The statistical geometry of an ideal two-dimensional fiber network. *Tappi* 1960; 43: 737–752.
[11] Nave, CR. HyperPhysics. Instructional material in physics (http://hyperphysics.phy-astr.gsu.edu). Department of Physics and Astronomy, Georgia State University, Atlanta USA, 2010.
[12] Mandl, F. *Statistical Physics*, 2nd ed. Chichester: John Wiley & Sons, 1988.
[13] Blatt, FJ. *Modern Physics*. McGraw-Hill, 1992.
[14] Zhurkov, SN. Kinetic concept of the strength of solids. *Int J Fracture Mech* 1965; 1: 311–323.
[15] Stepanov, WA, Peschanskaya, NN, Shpeizman, VV and Nikonov, GA. Longevity of solids at complex loading. *Int J Fracture* 1975; 11(5): 851–867.

[16] Cox, HL. The elasticity and strength of paper and other fibrous materials. *Br J Appl Phys* 1952; 3: 72.
[17] Gradin, P, Nyström, S, Flink, P, Forsberg, S, and Stollmaier, F. Acoustic emission monitoring of light-weight coated paper. *J Pulp Paper Sci* 1997; 23(3): 113–118.
[18] Salminen, L. *Aspects of Fracture Processes in Paper*. PhD thesis. Helsinki University of Technology, Espoo, Finland, 2003.
[19] Shames, IH, and Dym, C. *Energy and Finite Element Methods in Structural Mechanics*. New York, USA: Hemisphere Publishing Corporation, 1985.
[20] MATLAB Version R2009b. The MathWorks Inc, Natick, MA, USA, 2009.
[21] Heyden, S. *Network Modelling for the Evaluation of Mechanical Properties of Cellulose Fibre Fluff*. PhD thesis. Lund University, Sweden, 2000.

Appendix

A structural bond connects two nodes, which are rigidly coupled, for two different structural fiber beam elements at a crossing and consists of two circular domains with a diameter equal to the fiber width h. The bond element [21] has vanishing thickness and the two circular domains are connected by shear springs having the stiffness k as schematically illustrated in Figure 14.

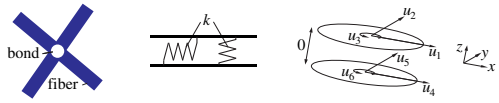

Figure 14. A structural bond consists of two circular domains connected by springs having stiffness k. The in-plane translational and rotational displacements in a Cartesian coordinate system xyz are given by u_1 to u_6.

The element stiffness matrix $\mathbf{K}_e$, having in-plane translational and rotational stiffness, is written as a standard 6×6 matrix:

$$\mathbf{K}_e = \begin{bmatrix} kA_b & 0 & 0 & -kA_b & 0 & 0 \\ 0 & kA_b & 0 & 0 & -kA_b & 0 \\ 0 & 0 & kI_p & 0 & 0 & -kI_p \\ -kA_b & 0 & 0 & kA_b & 0 & 0 \\ 0 & -kA_b & 0 & 0 & kA_b & 0 \\ 0 & 0 & -kI_p & 0 & 0 & kI_p \end{bmatrix},$$

where $A_b = \pi h^2/4$ is the cross-sectional area of the bond element and $I_p = \pi h^4/64$ is its polar moment of inertia.